

Short communication

Synthesis and Characterization of Mn₂O₃ nanorods as Anode Materials for Lithium Ion Batteries

Lei He^{1,2,*}, Chunguang Xu^{1,2,*}, Pengzhi Ma^{1,2}, Qiutao Wang^{1,2}

¹ School of Mechanical Engineering, Beijing Institute of Technology, Beijing 100081, China

² Fundamental Science on Advanced Machining Laboratory, Beijing 100081, China

*E-mail: heleibuaa@126.com, xucg@bit.edu.cn

Received: 2 February 2020 / Accepted: 22 March 2020 / Published: 10 May 2020

MnOOH nanorods were synthesized by a simple precipitation method employing manganese sulfate and potassium permanganate as raw materials and CTAB as surfactant and used as a precursor to prepare Mn₂O₃ nanorods. Comprehensive study of the structure and performance of the Mn₂O₃ nanorods was carried out by various physical and chemical experiments, such as ultrasound microscopy and electrochemical tests. According to X-ray diffraction, scanning electron microscopy and transmission electron microscopy observations, the Mn₂O₃ crystallizes very well and has a homogeneous rod morphology. The width and length of the nanorods were 200~300 nm and 2~4 μm, respectively. Further analysis of the electrode performance of the material revealed that it delivers a high second discharge capacity of 1005 mAh·g⁻¹ at 0.1C when used as an anode material for lithium-ion batteries.

Keywords: MnOOH; Anode materials; Mn₂O₃; Lithium ion battery.

1. INTRODUCTION

Due to the excessive use of traditional fuels (such as coal, oil, etc.) and increasing environmental pollution, developing renewable energy systems is a very urgent task. Efficient, clean and renewable electrochemical energy conversion devices can effectively realize the efficient conversion of clean energy sources; such devices include fuel cells, supercapacitors, and lithium-ion batteries (LIBs)[1]. LIBs are a rapidly growing and highly regarded energy storage technology that has been widely used in communications, transportation and renewable energy in recent years[2]. At present, graphite is the main anode material of LIBs because graphite has excellent endurance and sufficient storage and is comparatively inexpensive. However, the capacity of graphite anodes for typical LIBs is relatively low, only 370 mAh·g⁻¹ [3].

Recently, transition metal oxides (MO_x, M = Fe, Co, Ni, Mn, etc.) prepared through the conversion reaction $MO_x + 2xLi \rightleftharpoons M_{+x}Li_2O$ have been used for lithium storage. Transition metal oxides

have the advantages of a high theoretical capacity, good safety performance and low price and have been widely studied. However, the kinetic process of the oxide transformation reaction of transition metals is slow, and voltage hysteresis results in a relatively low working voltage and energy density. In addition, the conductivity of transition metal oxides is generally low. During the process of charge and discharge, a large volume change will occur, thus limiting the practical application of such materials in LIBs. Among the numerous transition metal oxides, Mn_2O_3 has a high specific theoretical capacity ($1018 \text{ mAh}\cdot\text{g}^{-1}$) and has been widely studied[4]. However, the material undergoes volume expansion in the process of charging and discharging, which leads to serious capacity attenuation. Therefore, much attention has been paid to enhancing the cycle performance and reducing the irreversible capacity[5-7]. Different morphologies and smaller particles of electrode materials can improve the electrochemical properties, especially for transition metal oxide materials.

In this study, the large-scale synthesis of γ - $MnOOH$ nanorods by a hydrothermal method and the conversion of the nanorods to Mn_2O_3 through a calcination process are reported. The process is simple and inexpensive for large-scale production. To further study the properties of the prepared materials as anode materials for LIBs, the prepared materials were assembled into coin batteries, and the effects of morphology and structure on electrochemical properties were studied by electrochemical performance testing.

2. EXPERIMENTAL

In this study, the required reagents, including CTAB (hexadecyl trimethyl ammonium bromide), $MnSO_4\cdot H_2O$ and $KMnO_4$, were of analytical reagent grade and were not further purified before use.

2.1. Synthesis of γ - $MnOOH$

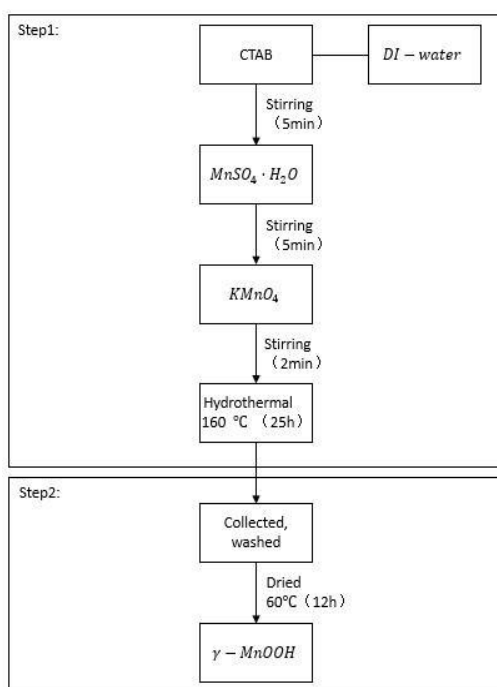


Figure 1. Synthesis flow diagram of γ - $MnOOH$ nanorods.

Step 1: CTAB (cetyltrimethylammonium bromide), $\text{MnSO}_4 \cdot \text{H}_2\text{O}$, and KMnO_4 were uniformly stirred in distilled water according to Fig. 1. Subsequently, the solution was poured into a vessel and kept at $160\text{ }^\circ\text{C}$ for hydrothermal reaction for 25 h.

Step 2: The sample was left to cool naturally to room temperature. The precipitate was collected from the vessel. The samples were washed several times and dried at $60\text{ }^\circ\text{C}$ for 12 h[8].

2.2. Conversion of $\gamma\text{-MnOOH}$ to Mn_2O_3

The obtained precipitate was calcined at $350\text{ }^\circ\text{C}$ in air for 1 h, and a black powder was collected.

2.3. Structural and morphological characterization

The crystal structure of the material was characterized by an X-ray diffraction instrument (Rigaku D/Max-2400, Japan). The X-ray source was Cu Ka, the scanning speed was 6° min^{-1} , and the scanning angle was $10^\circ\text{-}80^\circ$ (2θ). The material surface morphology was studied by field emission electron microscopy (Hitachi S-4800) and transmission electron microscopy. The electrode collector was made of aluminium foil and was cast into a slurry. The components were the active material, carbon black and PVDF at a ratio of 15:3:2 in the solvent N-methylpyrrolidinone. The as-fabricated electrodes were dried in vacuum at $60\text{ }^\circ\text{C}$ for 12 h. Then, the electrochemical properties of the materials were detected by a NEWARE battery test system (BTS-610). During detection, the current density at 1C was $1080\text{ mAh}\cdot\text{g}^{-1}$, and the voltage range for charge and discharge was 2.0 - 4.6 V.

3. RESULTS AND DISCUSSION

3.1 Material Characterization

The XRD pattern of single-crystal $\gamma\text{-MnOOH}$ is shown in Fig. 1a. It can be clearly observed that all diffraction peaks correspond exactly to the monoclinic structure of MnOOH , SGP21/c (No. 14), and the standard card (JCPDS No. 88-0649) [9] has the same value. The sharp and symmetric diffraction peaks in Fig. 1a indicate that the as-prepared $\gamma\text{-MnOOH}$ crystal has good crystallinity. Peaks from other phases were not observed, suggesting a high purity of $\gamma\text{-MnOOH}$.

FTIR spectroscopy has high sensitivity for the detection of low levels of organic-inorganic species. The sharp peaks at 446, 488 and 592 cm^{-1} correspond to the vibration of the Mn–O bonds in $\gamma\text{-MnOOH}$ [10,11], as shown in Fig. 2b. The representative peaks of the OH bending show good accordance with the experimental results at 1085, 1119 and 1152 cm^{-1} [12]. In addition, the peaks at 1630, 3440 and 2680 cm^{-1} are shown in Fig. 2b. These peaks could indicate the presence of a small amount of water and carbon dioxide [13]. Based on the above results, a chemical reaction formula was derived as shown in formula 3.1.



The material surface morphology was studied by FESEM and HRTEM, and the corresponding images are shown in Fig. 2c and Fig. 2d, respectively. The high-resolution FESEM image indicates that γ -MnOOH consists of six symmetrical arms extending from the centre. Based on the above analysis, the practical results confirm that the as-prepared single crystal γ -MnOOH has a good uniform morphology.

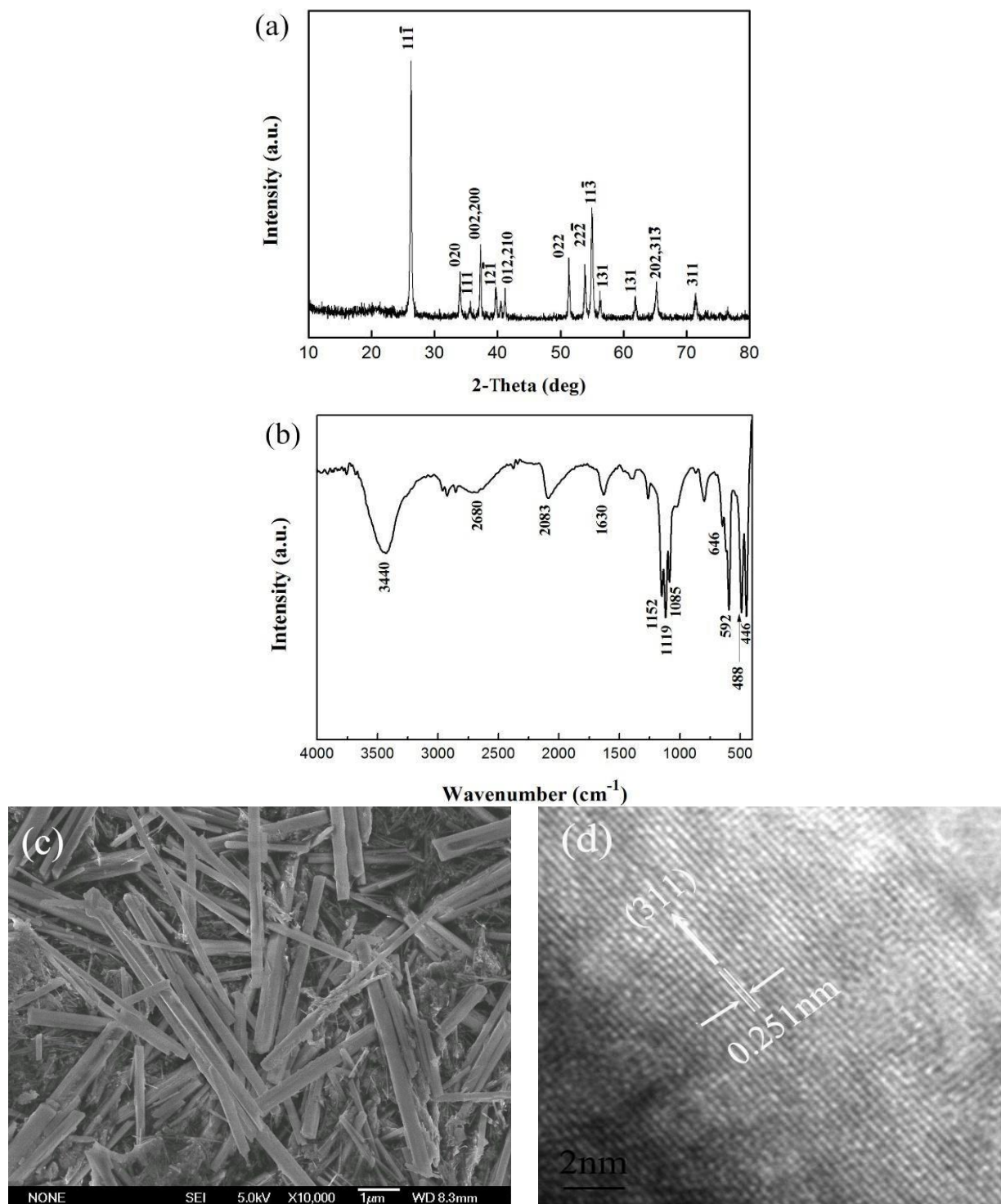


Figure 2. (a) XRD pattern of the obtained γ -MnOOH. (b) FTIR spectrum of as-prepared γ -MnOOH. (c) SEM image of as-prepared γ -MnOOH. (d) HRTEM image of as-prepared γ -MnOOH.

As seen from Fig. 3a., the 2θ angles of 23.1° , 32.9° , 38.2° , 45.2° , 49.3° , 55.2° , 64.1° , 65.8° and 67.5° correspond to the (211), (222), (400), (332), (431), (440), (541), (622) and (631) lattice planes, respectively. This result is consistent with the structure of cubic-phase Mn_2O_3 (JCPDS card No. 41-1442)[14]. There were no other peaks in the spectrum, indicating that the prepared material was pure Mn_2O_3 . Therefore, a chemical reaction formula was derived as shown in formula 3.2.



To study the effect of the precursor on the morphology and structure of the prepared material, the Mn_2O_3 samples were studied by SEM and TEM, as shown in Fig. 3b and Fig. 3c. As observed in Fig. 3b, the Mn_2O_3 powder had well-dispersed nanorods. The nanorod width and length were 200~300 nm and 2~4 μm , respectively. The nanorod morphology was similar in diameter to the precursor $\gamma\text{-MnOOH}$. The electrochemical performance of electrode materials is closely related to the particle size and the particle size distribution of the material. The nanorod structure was considered to facilitate the diffusion of Li^+ ions and electrode-electrolyte transmission in electrochemical reactions. Therefore, the prepared Mn_2O_3 nanorods are very promising for improving electrochemical performance.

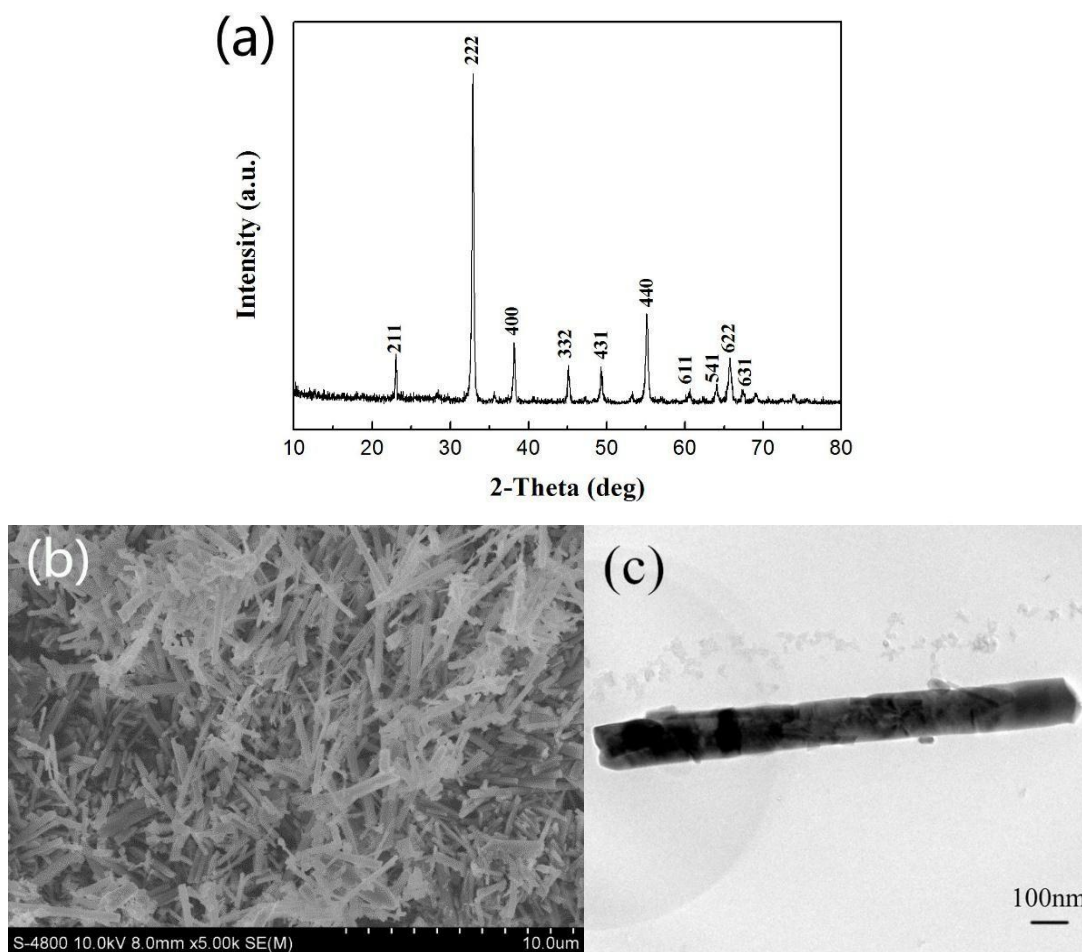
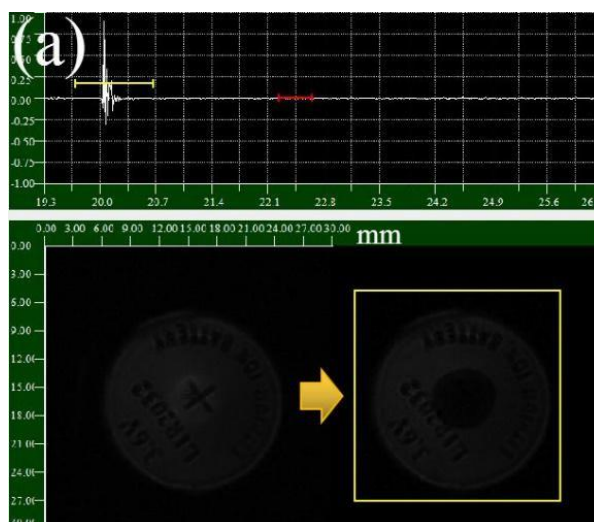


Figure 3. (a) XRD pattern (b) SEM image and (c) TEM image of Mn_2O_3 samples.

3.2 Electrochemical Characterization

To understand the electrochemical performance of Mn_2O_3 , a coin cell was assembled and tested. Fully equipped battery electrodes are shown in Fig. 4a. To better study the electrochemical behaviour of the Mn_2O_3 nanorods, we also observed their cycling performance, as shown in Fig. 4b. The as-prepared material had a high initial discharge capacity of $1060 \text{ mAh}\cdot\text{g}^{-1}$. The second discharge capacity reached $1005 \text{ mAh}\cdot\text{g}^{-1}$ at 0.1C. The discharge capacity exhibited large losses every 20 cycles, decreasing to $782 \text{ mAh}\cdot\text{g}^{-1}$ at the 20th cycle and $636 \text{ mAh}\cdot\text{g}^{-1}$ at the 40th cycle. There was a sudden jump to $706 \text{ mAh}\cdot\text{g}^{-1}$ at the 46th cycle, then the capacity continued to decline to $582 \text{ mAh}\cdot\text{g}^{-1}$ at 100 cycles. The capacity retention was 54.9% at a current density of 0.1C after 100 cycles. It is known from Tab. 1 that Mn_2O_3 has a promising theoretical specific capacity of $1018 \text{ mAh}\cdot\text{g}^{-1}$ and is superior to other excessive metal oxides. The electrochemical properties of other structures Mn_2O_3 were also compared. The electrochemical properties of the Mn_2O_3 nanorods are better than those reported in the previous literature. It is reported that the Mn_2O_3 nanowire anode delivers an initial discharge capacity of $815.9 \text{ mAh}\cdot\text{g}^{-1}$ at $100 \text{ mA}\cdot\text{g}^{-1}$ and maintains a capacity of $502.3 \text{ mAh}\cdot\text{g}^{-1}$ after 100 cycles in this literature [15-17]. Therefore, the one-dimensional nanorods structures provide short lithium-ion diffusion path, good charge transport, and volume flexibility for Li^+ intercalation/deintercalation, thus leading to good rate capability and cycling performance. The above electrochemical and cycle performance tests showed that the cells undergo an activation reaction where the capacity is higher than the theoretical capacity in the first cycle and have relatively stable performance from the 50th to 100th cycle. A possible cause for this behaviour may be that a portion of the material transforms to a spinel-like phase with increasing cycle number [18]. This phenomenon is attributed to the Jahn-Teller effect of active Mn^{3+} ions. Therefore, the gradual reduction in discharge capacity is partly due to structural transformation during electrochemical cycling.



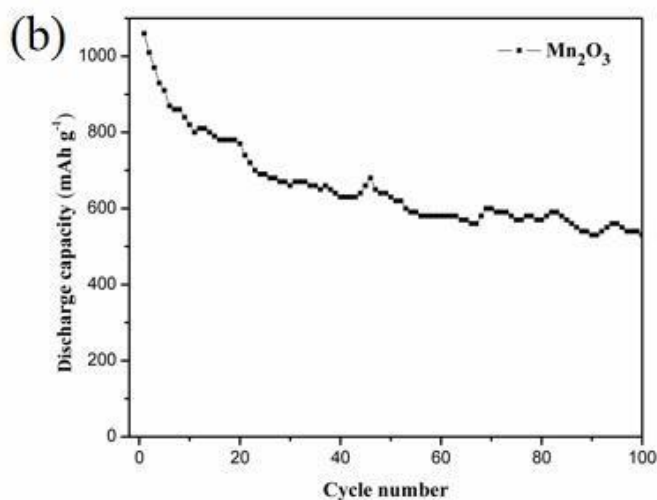


Figure 4. (a) Ultrasonic microscope pictures of the coin cell. (b) Electrochemical behaviour of the Mn_2O_3 nanorods.

Table 1. Comparison of the discharge capacity of transition metal oxides and similar materials when used as anode materials for LIBs.

Anode materials	SnO_2 ^[15] Hierarchical nanostructure	Mn_2O_3 ^[16] Porous Microsphere	Mn_2O_3 ^[17] nanowire	Mn_2O_3 nanorods
Theoretical specific capacity ($\text{mAh}\cdot\text{g}^{-1}$)	782	755	1018	1018
The initial discharge capacity ($\text{mAh}\cdot\text{g}^{-1}$)	516	925	815.9	1060
The discharge capacity after 100 cycles ($\text{mAh}\cdot\text{g}^{-1}$)	Serious attenuation	565	502.3	582

4. CONCLUSIONS

To summarize, Mn_2O_3 nanorods were synthesized by a simple and efficient method. The initial capacity of the Mn_2O_3 nanorods is $1060 \text{ mAh}\cdot\text{g}^{-1}$, and a high capacity of $582 \text{ mAh}\cdot\text{g}^{-1}$ is maintained after 100 cycles at 0.1C. These results clearly show that the Mn_2O_3 nanorods have a high specific capacity, long cycle life, good rate capability and good electrochemical performance, making them an ideal choice for LIBs. In addition, this research is expected to provide theoretical support for the development of anode materials and to be generalizable to other excellent anode materials for high-performance power batteries.

ACKNOWLEDGEMENTS

This work was supported by the National Natural Science Foundation of China (Grant No. 51335001 and U1737203). Ultrasonic nondestructive testing and high energy acoustic beam in-situ control of residual stress distribution in aeronautic aluminium alloy structures of weak rigidity.

References

1. P.P. Liu, Y.Q. Zheng, H.L. Zhu and T.T. Li, *ACS Appl. Nano Mater.*, 2 (2019) 744–749.
2. Z.Y. Wang, L. Zhou and X.W. Lou, *Adv. Mater.*, 24 (2012) 1903-1911.
3. Y.M. Sun, X.L. Hu, W. Luo, F.F. Xia and Y.H. Huang, *Adv. Funct. Mater.*, 23 (2013) 2436-2444.
4. Y.G. Guo, J.S. Hu and L.J. Wan, *Adv. Mater.*, 20 (2008) 2878-2887.
5. G. Prieto, H. Tüysüz, N. Duyckaerts, J. Knossalla, G.H. Wang and F. Schüth, *Chem. Rev.*, 116(22) (2016) 14056-14119.
6. Y. Xia, Z. Xiao, X. Dou, H. Huang, X.H. Lu, R.J. Yan, Y.P. Gan, W.J. Zhu, J.P. Tu, W.K. Zhang and X.Y. Tao, *ACS Nano*, 7(8) (2013) 7083-7092
7. W. Zhang, J.N. Li, J. Zhang, J.Z. Sheng, T. He, M.Y. Tian, Y.F. Zhao, C.J. Xie, L.Q. Mai and S.C. Mu, *ACS Appl. Mater. Interfaces*, 9(14) (2017) 12680-12686
8. L. He, S.C. Zhang, X. Wei, Z.J. Du, G.R. Liu and Y.L. Xing, *J. Power Sources*, 220 (2012) 228-235
9. N. Chandra, S. Bhasin, M. Sharma and D. Pal, *Mater. Lett.*, 61 (2007) 3728–3732
10. R.Z. Yang, Z.X. Wang, L. Dai and L.Q. Chen, *Mater. Chem. Phys.*, 93 (2005) 149-153.
11. W.X. Zhang, Z.H. Yang, Y. Liu, S.P. Tang, X.Z. Han and M. Chen, *J. Cryst. Growth*, 263 (2004) 394-399.
12. P.K. Sharma and M.S. Whittingham, *Mater. Lett.*, 48 (2001) 319-323.
13. Y.C. Zhang, T. Qiao, X.Y. Hu and W.D. Zhou, *J. Cryst. Growth*, 280 (2005) 652-657.
14. W.Y. Li, J.J. Shao, Q. Liu, X.J. Liu, X.Y. Zhou and J.Q. Hu, *Electrochim. Acta*, 157 (2015) 108–114.
15. H.B. Wu, J.S. Chen, X.W. Lou and H.H. Hng, *J. Phys. Chem. C*, 2011, 115, 50, 24605-24610.
16. H. Zheng, T. Wang, J.S. Chen, Q. Liu, R.F. Zhao and L. Li, *Mater. Sci. Eng.*, 274 (2017) 012162-012168.
17. Y.H. Wang, Y.H. Wang, D.S. Jia, Z. Peng, Y.Y. Xia and G.F. Zheng, *Nano Lett.*, 14 (2014) 1080–1084.
18. Y.G. Guo, J.S. Hu and L.J. Wan, *Adv. Mater.*, 20 (2008) 2878-2887.

© 2020 The Authors. Published by ESG (www.electrochemsci.org). This article is an open access article distributed under the terms and conditions of the Creative Commons Attribution license (<http://creativecommons.org/licenses/by/4.0/>).